

## A SUBHALO-GALAXY CORRESPONDENCE MODEL OF GALAXY FORMATION

JUHAN KIM<sup>1,2</sup>, CHANGBOM PARK<sup>1,3</sup>, AND YUN-YOUNG CHOI<sup>1,4</sup>

*October 25, 2018: Not to appear in Nonlearned J., 45.*

### ABSTRACT

We propose a model of allocating galaxies in cosmological N-body simulations. We identify each subhalo with a galaxy, and assign luminosity and morphological type assuming that the galaxy luminosity is a monotonic function of its host subhalo mass. The morphology assignment is made by using two simple relations between subhalo mass and galaxy luminosity of different types. One is using a constant ratio in luminosity of early (E/SO) and late (S/Irr) type galaxies at a fixed subhalo mass. And the other assumes that galaxies of different morphological types but having an equal luminosity have a constant ratio in their subhalo masses. We made a series of comparisons of the properties of these simulated galaxies with those of the SDSS galaxies. The resulting simulated galaxy sample is found to successfully reproduce the observed local number density distribution except for in high density regions. The luminosity function is studied as a function of local density. It was found that the observed luminosity functions in different local density environments are overall well-reproduced by the simulated galaxies. Discrepancy is found at the bright end of the luminosity function of early types in the underdense regions and at the faint end of both morphological types in very high density regions. A significant fraction of the observed early type galaxies in voids seems to have undergone a relatively recent star formation and became brighter. The lack of faint simulated galaxies in dense regions may be due to the strong tidal force of the central halo which destroys less massive satellite subhalos around in the simulation. The mass-to-light ratio is found to depend on the local density in the way similar to that observed in the SDSS sample. We have found an impressive agreement between out simulated galaxies and the SDSS galaxies in the dependence of the central velocity dispersion on the local density and luminosity.

*Subject headings:* Cosmology: simulation: halo-galaxy: luminosity function: Numerical

### 1. INTRODUCTION

The current galaxy formation paradigm can be characterized by “hierarchical clustering”. This means that massive dark matter halos form by merging less massive halos and/or by accreting ambient matter, and also that a dark matter halo governs the evolution of the galaxy residing inside. Most galaxies are believed to be hosted by the dark matter halos because the halos can provide a deep potential well for baryonic matter to condense and cool down. This leads to triggering of the star formation; gas sufficiently accumulated in the halo potential center begins to experience many hydrodynamic processes, such as radiative cooling, star-formation, supernova explosion, and chemical enrichments. All of these processes play an important role in making the visible galaxies in the end. Because galaxies as a building block of the large scale structures consequently follows the evolution of their host halos over the cosmic history, understanding gravitational evolution of dark halos is very important for the study of galaxy formation and evolution.

Over the past few decades, cosmological simulations have been proved useful for the study of structure formation. Simulations have boosted up many investigations of the nonlinear structure evolutions and their results have been extensively compared to the observations in various aspects of interest. Many studies

have reported successful recovery of observational features of the galaxy distribution like the two-point correlations of galaxies (Conroy et al. 2006; Kravtsov et al. 2004; Berlind & Weinberg 2002), topology (Park et al. 2005a,b; Gott et al. 2006), and the environmental dependence of spin distributions (Cervantes-sodi et al. 2007).

Detailed modeling of galaxy evolution and understanding of the galaxy properties have been possible with the recent advent of the huge redshift surveys such as Sloan Digital Sky Survey<sup>5</sup> (SDSS) and 2dFGRS<sup>6</sup>. These larger surveys provide a rich information on the formation and evolution of galaxy. To meet a requirement to establish a relation between simulated structures and observed galaxies many techniques have been introduced. The semi-analytic model(SAM) of galaxy formation (Cole et al. 1994; Kauffmann et al. 1997; Baugh 2006) is based on the hierarchical clustering of halos whose merging history trees are built by generating a set of Gaussian random numbers. The mass growth history of halos on various mass scales can be generated and traced by this method. Numerous SAM parameters are implemented in the merging history to reflect the hydrodynamical processes of heating, cooling, star formation, and aging the stellar populations. Their parameter values are fine tuned for the best description of collective properties of observed galaxies. But as the number of observational constraints increases, the number of parameters increases and the SAM becomes much complicated. Hydro simulations employ direct formulations of the

<sup>1</sup> Korea Institute for Advanced Study, Hoegiro 87, Dongdaemun-Gu, Seoul, 130-722, Korea

<sup>2</sup> kjhan@kias.re.kr

<sup>3</sup> cbp@kias.re.kr

<sup>4</sup> yychoi@kias.re.kr

<sup>5</sup> <http://www.sdss.org>

<sup>6</sup> <http://www.aao.gov.au/2df/>

hydrodynamic processes (Weinberg et al. 2006). Two types of hydro simulations are now widely adopted; the Lagrangian (Monaghan 1992; Hernquist & Katz 1989) and Eulerian methods (Tasker & Bryan 2006; Harten, A. 1997, and for comparative study, see Heitmann et al. 2005; Thacker et al. 2000). They set gas particles or gas grids in the system of interest. Then, gas dynamics are taken into account by calculating the hydrodynamic interactions between neighbor particles or by solving differential hydro equations between adjacent grids. This method has several weak points; it suffers from the lack of resolutions in space and mass as the N-body simulations. And in most cases, the star formation and supernova explosions are far beyond the simulation resolution. Some processes such as radiative transfer, star formation, supernovae feedback, and initial stellar mass function, are not thoroughly understood and are difficult to parameterize in a well established way.

One of the offsprings of the SAM is the Halo Occupation Distribution (HOD; Zheng et al. 2005; Seljak 2000; Berlind & Weinberg 2002) model. It relates the Friend-of-Friend (FoF) halo mass to the number of contained subhalos (or galaxies) using a conditional probability,  $P(N|M)$ , where  $M$  is the FoF halo mass and  $N$  is the number of subhalos inside the FoF halo. This probability function is obtained from numerical simulations (Kravtsov et al. 2004; Berlind & Weinberg 2002; Jing et al. 1998) or from observations (Zehavi et al. 2004; Abazajian et al. 2005; Zheng et al. 2007) fitting the model to the observed two-point correlation functions.

Another variant of the SAM is a one that adopts the one-to-one monotonic correspondence between the galaxy luminosity and subhalo mass (Marinoni & Hudson 2002; Vale & Ostriker 2004, 2006; Shankar et al. 2006). This method is often called the ‘‘correspondence model’’. It is simpler than other methods because it requires only two prerequisites; the luminosity function of galaxies and mass function of subhalos. Its key assumption that a more massive subhalo hosts a brighter galaxy, is consistent with the hierarchical clustering picture. As the halo mass grows, its luminosity is expected to grow in general because merging of halos may be followed by the merging of galaxies. By matching these two functions, the subhalo mass is mapped to galaxy luminosity.

However, sometimes a galaxy may survive the merger event because baryonic component of a galaxy is usually more concentrated and is more tightly bound than its dark counterpart. These ‘‘orphan’’ galaxies (Gao et al. 2004) which have no separate corresponding halos could exist in the cluster regions. Also halos of mass below a certain characteristic scale are unable to provide baryonic matter with gravitational attraction strong enough to resist against supernova explosions which can tear up the small-mass system. Even though such cases are many, it is sound to expect that the galaxy census is closely related to the population of subhalos because most of the observed galaxies are field galaxies who have their own dark halos. It is worth investigating the hypothesis of the subhalo-to-galaxy correspondence model of galaxy formation.

In this paper, we apply the subhalo-galaxy correspondence model to a large N-body simulation and compare

the statistical properties of simulated galaxies with those of galaxies observed by the SDSS. We organize this paper as follows. In section 2 we describe our simulation and the subhalo finding method. In section 3, we implement the subhalo-galaxy correspondence model and show how to assign morphological types to mock galaxies. In section 4, the local density is introduced to quantify local environments and the local density distributions of mock and SDSS galaxies are investigated. We also compare the luminosity distribution of simulated galaxies with those of the SDSS galaxies in section 5. The environmental dependence of central velocity distributions are studied for the mock and SDSS galaxies in section 6. And discussions and conclusions follow in section 7.

## 2. SIMULATION AND HALO FINDING

We have carried out a cosmological N-body simulation of the universe with the WMAP 3-year cosmological parameters. We ran  $1024^3$  cold dark matter particles using an improved version of the GOTPM code (Dubinski et al. 2004). The code adopts a dynamical domain decomposition for the Particle-Mesh part with a variable width of the z-directional domain slabs. It also uses more compact and efficient oct-sibling tree walks reducing the computational cost for the short-range force update which consumes about 90 % of total run time. As a results, this new version outperforms the previous version by about factor three in speed. The simulation was run on a beowulf-type system installed at Korea Institute for Advanced Study. The linux cluster consists of 256 AMD cores and 1 tera-byte main memory.

The simulation and cosmological parameters adopted in this study are lists in Table 1. The number of time steps in the simulations are empirically pre-determined to satisfy the requirement that the maximum displacement of particles in a step should be less than the force resolutions which is 0.1 times the mean interparticle separation ( $d_{\text{mean}}$ ). The starting epochs of simulations are chosen to constrain that any particle should not overshoot neighbors when the Zel’dovich displacement is made.

Subhalos are identified by the PSB method (Kim & Park 2006). The method applies the FoF algorithm to identify dark matter particle groups adopting the standard linking length,  $l_{\text{link}} = 0.2d_{\text{mean}}$ . Then it divides each FoF halo into subhalos. This two-stage halo finding is in common with other methods (Springel et al. 2001; Shaw et al. 2006). In the second stage we build a particle density field by a coordinate-free method as usually adopted in the smoothed particle hydrodynamics (Monaghan 1992). This adaptive kernel implementation is intended to resolve tight clusterings of particles. Then, we search for 26 nearest neighbors at each particle. To construct isodensity contour we move along the neighbor positions in a similar way used in the original PSB method (for details see Kim & Park 2006). Self-bound and tidally stable subhalos are identified by measuring the tidal radius of the subhalos and total energies of their member particles; member candidates are selected if their distances to the center of a subhalo are less than tidal radius of the subhalo. Among these particles, gravitationally unbound particles are discarded. The resulting subhalos are used to allocate galaxies. We call the most massive subhalo a central halo and other

subhalos satellite halos in the FoF group. Also, the group of particles found by the FoF method are named the FoF group or FoF halo.

### 3. THE SUBHALO-GALAXY CORRESPONDENCE MODEL

We use the monotonic one-to-one correspondence model between galaxies and subhalos; there is one and only one galaxy in each subhalo and a more massive subhalo hosts a more luminous galaxy. We apply this model to assign galaxies within our simulation box.

The one-to-one correspondence model is formalized in the following way. We first measure the mass function  $\Phi(M_h)$  of PSB subhalos. We then take the observed luminosity functions of the early (E/S0) and late (S/Irr) type galaxies. The relation between the halo mass and the corresponding absolute magnitude limits is given by the following integral equation.

$$\int_{M_h}^{\infty} \Phi(M') dM' = \int_{-\infty}^{\mathcal{M}_E(M_h)} \phi_E(\mathcal{M}') d\mathcal{M}' + \int_{-\infty}^{\mathcal{M}_L(M_h)} \phi_L(\mathcal{M}') d\mathcal{M}', \quad (1)$$

where  $\Phi$  is the subhalo mass function and  $\phi_E$  and  $\phi_L$  are the luminosity functions of early and late type galaxies. In this equation we separate the full luminosity function of subhalos into those of early and late types to take into account the difference in mass of the halos associated with galaxies of different morphological type.

Two models are proposed to utilize the simple mass and luminosity scaling ratios between different morphological types at the fixed luminosity and at the fixed mass, respectively. The first model uses

$$L_L(M_h) = L_E(\kappa M_h), \quad (2)$$

where  $M_h$  is the subhalo mass, and  $L_L$  and  $L_E$  are the luminosities of late and early types, respectively. The equation means that at an equal luminosity the early type galaxy is  $\kappa$  times more massive than the late type galaxy. This model is based on the findings of Park et al. (2007a) who have assured that the early type galaxies brighter than  $M_r = -19.5$  have about  $\sqrt{2}$  times higher central velocity dispersion and pairwise peculiar velocity difference compared to the late types of the same brightness. This implies  $\kappa \approx 2$  if  $(M_h/L)_E = \kappa(M_h/L)_L$ . Another convincing observational evidence for  $\kappa = 2$  can be also found in Mandelbaum et al. (2006) who obtained the same result for halos of mass greater than  $10^{11} h^{-1} M_\odot$  from the analysis of the galaxy-galaxy weak lensing of the SDSS sample. Equation (2) then makes equation (1) a one-to-one relation between halo mass and galaxy luminosity. From now on, we name it  $\kappa$  model. The second model uses a constant factor for the luminosity rather than the mass. This relation can be formulated as

$$L_L(M_h) = \beta L_E(M_h), \quad (3)$$

which says that late type galaxies are brighter than early type galaxies of the same mass by a factor of  $\beta$ . Now we call it the  $\beta$  model.

For the galaxy luminosity distribution, we use the Schechter function

$$\phi(\mathcal{M}) = (0.4 \ln 10) \phi^* 10^{-0.4(\mathcal{M}-\mathcal{M}^*)(\alpha+1)} \exp\left[-10^{-0.4(\mathcal{M}-\mathcal{M}^*)}\right], \quad (4)$$

where we adopt the type-specific Schechter function parameters  $\mathcal{M}_E^* - 5 \log_{10} h = -20.23$ ,  $\phi_E^* = 7.11 \times 10^{-3} h^3 \text{Mpc}^{-3}$ , and  $\alpha_E = -0.53$  for early type galaxies and  $\mathcal{M}_L^* - 5 \log_{10} h = -20.12$ ,  $\phi_L^* = 12.27 \times 10^{-3} h^3 \text{Mpc}^{-3}$ , and  $\alpha_L = -0.90$  for late types in the  $r$  band, which are given in Table 2 of Choi et al. (2007) for the SDSS galaxies brighter than  $\mathcal{M}_r = -19.0$  (Hereafter, we will drop the term  $5 \log_{10} h$  in the absolute magnitude and the magnitudes are all  $r$ -band magnitude.) These parameter values are quite different from those given by Blanton et al. (2001) and Blanton et al. (2003) mostly because we are using the type-specific functions. Reducing the effects of the internal extinction by Choi et al. also makes a significant difference in the  $\alpha$  parameter compared to Blanton et al.'s results. Difference also comes from the data size (Dr4plus versus  $\sim$ DR1), adopted cosmology ( $\Omega_m = 0.27$ ,  $\Omega_\Lambda = 0.73$  versus  $\Omega_m = 0.3$ ,  $\Omega_\Lambda = 0.7$ ), and sample definition (volume-limited versus apparent magnitude-limited).

The  $\beta$  model can be easily solved by using the relation,  $\mathcal{M}_L(M_h) = \mathcal{M}_E(M_h) - 2.5 \log_{10} \beta$  in equation (1), but the  $\kappa$  model is a bit tricky to solve and needs a few assumptions. The  $\kappa$  model can be solved by a chain of equations whose  $n$ -th term is,

$$\int_{M_h/\kappa}^{M_h} \Phi(M) dM = \int_{\mathcal{M}_{n-2}}^{\mathcal{M}_{n-1}} \phi_L(\mathcal{M}) d\mathcal{M} + \int_{\mathcal{M}_{n-1}}^{\mathcal{M}_n} \phi_E(\mathcal{M}) d\mathcal{M}, \quad (5)$$

where  $\mathcal{M}_{n-2} \leq \mathcal{M}_{n-1} \leq \mathcal{M}_n$  and

$$M_h(\mathcal{M}_{L,n-2}) = M_h(\mathcal{M}_{E,n-1}) \equiv m \quad (6)$$

$$M_h(\mathcal{M}_{L,n-1}) = M_h(\mathcal{M}_{E,n}) = m/\kappa, \quad (7)$$

for  $\kappa > 1$ . Here  $M_h(\mathcal{M}_L)$  and  $M_h(\mathcal{M}_E)$  denote the halo masses of late type and early type galaxies of absolute magnitude  $\mathcal{M}$ , respectively. If  $M_h$ ,  $\mathcal{M}_{n-2}$ , and  $\mathcal{M}_{n-1}$  are given, then  $\mathcal{M}_n$  can be derived. Figure 1 depicts the relations among the three magnitudes described above. The solid and dashed curves show the luminosity functions of early and late types, respectively. And the dotted line connects the same mass of the two morphological types. The shaded areas denoted by  $A_n$  and  $B_n$  are the integrated number densities of galaxies of magnitude between  $\mathcal{M}_{n-2}$  and  $\mathcal{M}_{n-1}$  for the late type and between  $\mathcal{M}_{n-1}$  and  $\mathcal{M}_n$  for the early type, respectively. Therefore, the sum of the two shaded areas should be equal to the integrals of the subhalo mass function (the left-hand side of Eq. 5). By making a stride to the next mass scale which is smaller by  $1/\kappa$  times, we can get a chain of equations and derive the scaling relation between the mass and the luminosity. To solve this chain of equations we set initial conditions under the plausible assumption that the late-type contributions to the number density at the high-mass (or bright) end are negligible compared to those of early types (or  $0 \simeq A_1, A_2 \ll B_1, B_2$ ). This setting is quite fair from the fact that early type galaxies dominate the bright end population of galaxies. Then, we are able to solve the series of equation (5) from the initial conditions where only the early-type contribution to number density is dominant.

Now we investigate the early type fractions as a function of the host subhalo mass. The probability of a

TABLE 1  
 SIMULATION PARAMETERS

name	$N_p$	$N_m$	$L_{box}^a$	$N_{step}$	$z_i$	$h$	$\Omega_m$	$\Omega_b$	$\Omega_\Lambda$	$n_s^b$	$b$	$m_p^c$	$\epsilon^d$
H2	$1024^3$	$1024^3$	256	3800	95	0.732	0.238	0.042	0.762	0.958	1.314	$1.0 \times 10^9$	$25h^{-1}\text{kpc}$

<sup>a</sup> in  $h^{-1}\text{Mpc}$

<sup>b</sup> spectral power index

<sup>c</sup> particle mass in  $h^{-1}M_\odot$

<sup>d</sup> force resolution

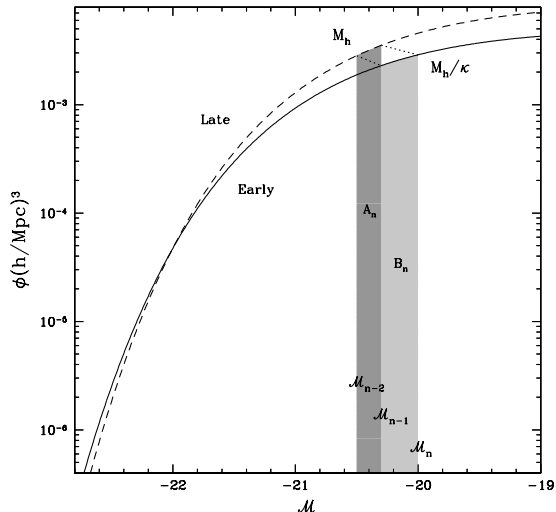


FIG. 1.— Illustration to derive the  $M_h$ – $M_r$  relation for the  $\kappa$ . The solid and dashed curves are the luminosity functions of early and late type galaxies, respectively. And the dotted line connects the same mass of the two types. The shaded areas tagged by  $A_n$  and  $B_n$  are the numbers of galaxies in the magnitude intervals between  $\mathcal{M}_{n-2}$  and  $\mathcal{M}_{n-1}$  for the late type and between  $\mathcal{M}_{n-1}$  and  $\mathcal{M}_n$  for the early type, respectively.

galaxy of mass  $M_h$  to be early type is given by

$$f_E(M_h) = \frac{\phi_E(\mathcal{M}_E|M_h)}{\phi_E(\mathcal{M}_E|M_h) + \phi_L(\mathcal{M}_L|M_h)}, \quad (8)$$

where the denominator is the luminosity function of all galaxies of mass  $M_h$  and the numerator is the luminosity function of early types of mass  $M_h$ . Figure 2 shows the results for the  $\kappa$  and  $\beta$  models. Using  $f_E$  we are able to randomly assign morphological type to each mock galaxy in accordance with its halo mass. For a larger value of  $\beta$ , the early type galaxy tends to dominate the population down to lower mass scales ( $M_c$ ) and below  $M_c$   $f_E$  drops more rapidly. But for the  $\kappa$  model, those changes in  $f_E$  are not so much steep. Also, in this plot, we note that a more dramatic change of the  $f_E$  in the  $\beta$  model than the  $\kappa$  model.

Figure 3 shows the relation between the subhalo mass  $M_h$  and absolute magnitude  $M$  of early (*solid lines*) and late (*dashed lines*) type galaxies derived from equation (1) and the luminosity functions of the SDSS galaxies in the  $\kappa$  (*upper*) and  $\beta$  (*lower panels*) models. Only shown are the cases of  $\beta = 2$  (thick lines) and 1.5 (thin lines) and  $\kappa = 2$  (thick lines) and 3 (thin lines). For a comparison, the characteristic minimum mass of the central subhalos at each absolute magnitude limit estimated by Zheng et al. (2007) based on the HOD model is given as filled circles. They obtained the magnitude-to-mass relation of the central subhalo but ignored the morphological types of galaxies. The HOD model is quite consistent with our

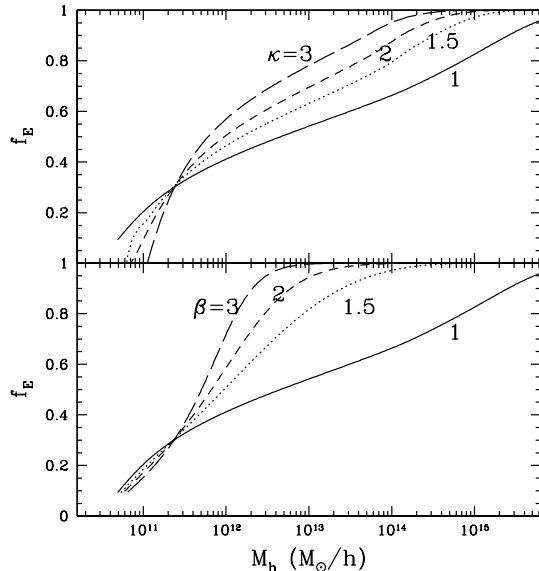


FIG. 2.— Early type fractions as a function of host subhalo mass. Each curve shows the fractional distributions of early type galaxies for  $\beta = 1, 1.5, 2,$  and  $3$  (*lower panel*) and for  $\kappa = 1, 1.5, 2,$  and  $3$  (*upper panel*) models. The model parameter values are attached to the curves.

$M_h$ – $M$  relation for the early type galaxies with  $\beta = 2,$  and  $\kappa = 2$  and  $3$ .

In the lower panel of Figure 4 shows the mass versus luminosity relation (solid line) for the early type galaxies. Here we adopt  $\mathcal{M}_\odot = 4.64 - 5 \log_{10} h$  (Blanton & Roweis 2006) to transform the magnitude to luminosity in the  $r$ -band filter. It can be noted that galaxy luminosity drops steeply at the low mass end and rises in a power law at the high mass end. Taking into account these features, we propose a function

$$L(M) = \frac{M^*}{\Psi_{ml}} \left( \frac{M^*}{M} \right)^{\gamma-1} e^{-\left(\frac{M^*}{M}\right)}, \quad (9)$$

as a fitting function for the halo mass versus early-type galaxy luminosity relation. We apply the  $\chi$ -square fitting to the relation and obtain the best-fit parameter values of  $\Psi_{ml} = 38.3hM_\odot/L_\odot$ ,  $M^* = 2.04 \times 10^{11}h^{-1}M_\odot$ , and  $\gamma = 0.644$  for the early type in the  $\beta = 2$  model. In the  $\kappa = 2$  model,  $\Psi_{ml} = 39.8(20.3)hM_\odot/L_\odot$ ,  $M^* = 4.83(1.52) \times 10^{11}h^{-1}M_\odot$ , and  $\gamma = 0.667(0.719)$  for early (late) type. Only the fitting result for the early type in the  $\beta = 2$  model is shown by a short-dashed line. The top panel shows the mass-to-light ratios of the early (solid curve) types in the  $\beta = 2$  model. The long-dashed and dotted curves show those ratios of early and late type galaxies in the  $\kappa = 2$  model. In the  $\beta = 2$  model, there is a upturn of the mass-to-light ratio of early types around  $M_h = 3 \times 10^{11}h^{-1}M_\odot$  (for those measured in other bands, see van den Bosch et al. 2003; Yang et al.

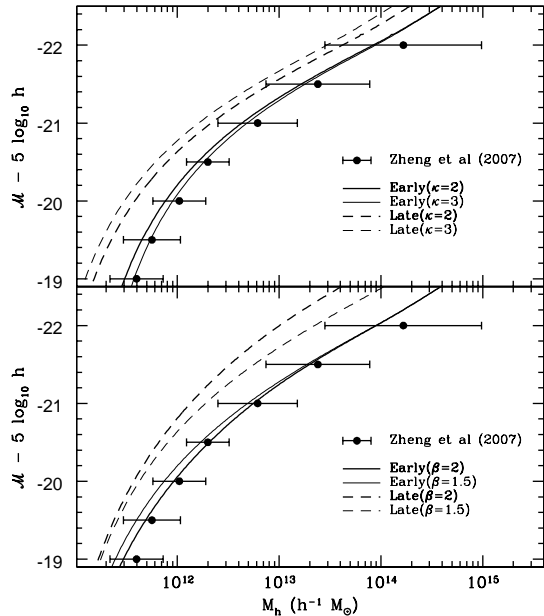


FIG. 3.— Scaling relation between halo mass and galaxy magnitude in the  $\kappa$  (upper panel) and  $\beta$  (lower panel) models. In the lower panel, *solid* lines shows the dependence of the modeled early type magnitude on the host subhalo mass for  $\beta = 2$  (*thick*) and for  $\beta = 1.5$  (*thin*). And in the upper panel, we show the mass-to-magnitude relations for  $\kappa = 2$  (*thick*) and  $\kappa = 3$  (*thin*) models. *Dashed* curves show the relations of late type galaxies. Filled circles are the best-fitting results of the SDSS observations to the HOD model in Zheng et al. (2007). And the errorbar is the width of the cut-off profile of the step-like function in the HOD model (for details, please see their paper).

2003; Eke et al. 2006), which means the star formation in galaxies is strongest at the mass scale. A fitting formula for the mass-to-light ratio is derived from equation (10),

$$\Upsilon \equiv M/L = \Psi_{ml} \left( \frac{M}{M^*} \right)^\gamma e^{\left( \frac{M^*}{M} \right)}. \quad (10)$$

Using this equation, the mass scale corresponding to the minimum mass-to-light ratio can be related to the shape parameters as  $M_u = M^*/\gamma$  and the minimum mass-to-light ratio is  $\Upsilon_u(E) = \Psi_{ml}(e/\gamma)^\gamma \simeq 100$  for early type galaxies and  $\Upsilon_u(L) \simeq 50$  for late types in the  $\beta = 2$  model.

According to our result the mass-to-light ratio of the brightest galaxies reaches much higher than  $10^3$ . But this value is too high compared to those reported in literature. For example, Mandelbaum et al. (2006) noted that a mass-to-light of early types reaches  $M_h/L_r = 674$  for their brightest samples ( $-22.5 \leq \mathcal{M} \leq -22$  in Tab. 4 of their paper) of the SDSS lensing galaxies. The discrepancy may be explained by the fact that they are typically the brightest cluster galaxies. In our PSB halo identification method all mass not assigned to satellite galaxies is assigned to the central subhalo after the boundness check, which makes the central subhalo as massive as the whole cluster and their mass-to-light ratio very large (*cf.* Fig. 10 in Vale & Ostriker 2006 and Fig. 4 in Tinker et al. 2005). Then, the group or cluster mass-to-light ratio is the one to be compared at the very high mass scales.

#### 4. ENVIRONMENTAL EFFECTS ON THE GALAXY DISTRIBUTION

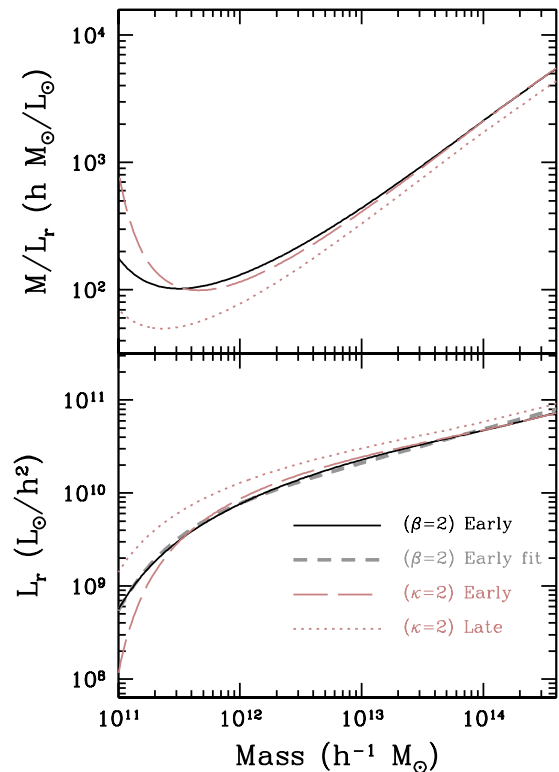


FIG. 4.— The scaling relation between the halo mass and the galaxy luminosity (lower panel) or mass-to-light ratio (upper panel) in the  $\beta = 2$  and  $\kappa = 2$  model. In the lower panel, the *solid* line shows the derived luminosity of early type mock galaxies as a function of the subhalo mass and the *short dashed* line is the best-fitting curve for it. Also the early (*long dashed*) and late (*dotted*) luminosity distributions are shown for the  $\kappa = 2$  model. In the upper panel, the mass-to-light ratio of the mock galaxies is shown by the line of the same type as shown in the lower panel. But we do not plot the fitting result in upper panel.

##### 4.1. Definition of the Local Density

For a comparative study of the environmental effects on the spatial and luminosity distributions of observed and simulated galaxies, a quantitative measure of the local environment is needed. To minimize the parameterizations and maximize the spatial resolution we use the spline kernel to obtain the smooth galaxy number density field. It is given by

$$W(q) = \begin{cases} (1 - \frac{3}{2}q^2 + \frac{3}{4}q^3) / (\pi h_s^3) & \text{for } 0 < q \leq 1, \\ (2 - q)^3 / (4\pi h_s^3) & \text{for } 1 < q \leq 2, \\ 0 & \text{otherwise,} \end{cases}$$

where  $q \equiv r/h_s$ . The kernel is centrally weighted more than the Gaussian, and has only one parameter,  $h_s$ . It is smooth to the second order and has a finite tail out to  $2h_s$ . Throughout this paper we set  $h_s = d_{20}/2$ , where  $d_{20}$  is the distance to the twentieth nearest neighbor galaxy. Due to these features and to the adaptive nature of  $h_s$  the resulting galaxy density map better represent the observed distribution of galaxies than the Gaussian, particularly in voids and clustered regions. To compare the observed and mock galaxy samples, it is necessary to make the number density of the density tracers the same. We use galaxies brighter than  $\mathcal{M} = -20$  as the galaxy density tracers. This selection differs slightly from that adopted by Park et al. (2007a) who chose  $-21 < \mathcal{M} < -20$ . We removed the bright cut

to better resolve the centers of clusters where galaxies brighter than  $L_*$  are concentrated.

#### 4.2. Number Density Distributions

The local density at galaxy positions is measured in our SDSS volume-limited samples. The density estimate is corrected for the boundary effects when the kernel sphere of radius  $d_{20}$  overlaps with the survey boundary. The late type galaxies having axis ratio  $b/a < 0.6$  are removed from the sample to reduce the effects of internal absorption on luminosity. After this exclusion, we give the weight of  $1/0.505$  to late type galaxies to correct the galaxy number density for the missing inclined ones, where  $0.505$  is the fraction of late types with  $b/a > 0.6$  in a sample containing galaxies down to  $\mathcal{M} = -17.5$  (the CM sample of Choi et al. 2007).

The correction for boundary effect is unnecessary for mock galaxies since their distribution is periodic in all directions. The redshift distortions effects caused by the peculiar velocities are mimicked by shifting the mock galaxies along the  $x$  axis using  $x' = x + v_x/H_0$ , where  $v_x$  is the  $x$ -component of peculiar velocity and  $H_0$  is the hubble constant.

Figure 5 shows the distribution of local density (*open circles*) at the location of galaxies in two volume-limited SDSS samples with absolute magnitude limits of  $-20.0$  (D5) and  $-18.5$  (D2) for the  $\beta = 2$  model. Also plotted are the local density distributions of simulated galaxies selected by the same magnitude-limit criteria. It can be noted that the local density distributions of the SDSS galaxies and the corresponding mock galaxies match closely to each other at all densities except for at high densities. Also those distributions for the  $\kappa = 2$  model are shown in Figure 6 with the same criteria.

Ostriker et al. (2003) employed a log normal function to fit the one-point distribution of dark matter density and luminosity density in their hydro-simulation. A spherical top-hat filter of constant radius is adopted in their study. They found a good agreement between the simulated density distributions and the log normal distribution while the distribution of luminosity density shows a poor fit. We check how well the galaxy density distribution, instead of dark matter or luminosity, is described by the non-normalized log normal function

$$\Xi(\Delta) \equiv \frac{dN(\Delta)}{d\log_{10} \Delta} = \frac{A}{\sqrt{2\pi}\sigma} e^{-(\ln \Delta - \mu)^2 / 2\sigma^2}, \quad (11)$$

where  $\Delta \equiv \rho/\bar{\rho}$  and  $A$  is the amplitude of the distribution. The mean number density of galaxies is  $n = A \log_{10} e$ . The best-fitting results are shown with dashed lines in each panel of Figure 5 and the fitting parameter values for various magnitude-limit ( $\mathcal{M}_{\text{lim}}$ ) samples are listed in Table 2. As can be noted, brighter galaxies tend to be located at higher local densities. Also the local density distribution becomes broader for brighter subsamples if viewed in the linear scale of overdensity or has nearly a constant width ( $\langle \sigma \rangle \simeq 1.29$ ) in log-scale.

Figure 7 and 8 shows the distribution of local density at locations of early (circles) and late (stars) type galaxies in the  $\beta = 2$  and  $\kappa = 2$  models, respectively. Open symbols are for the SDSS samples and the rest are for the simulated galaxies. The local density distributions of the simulated early and late type galaxies are very well matched with observations at low and intermediate

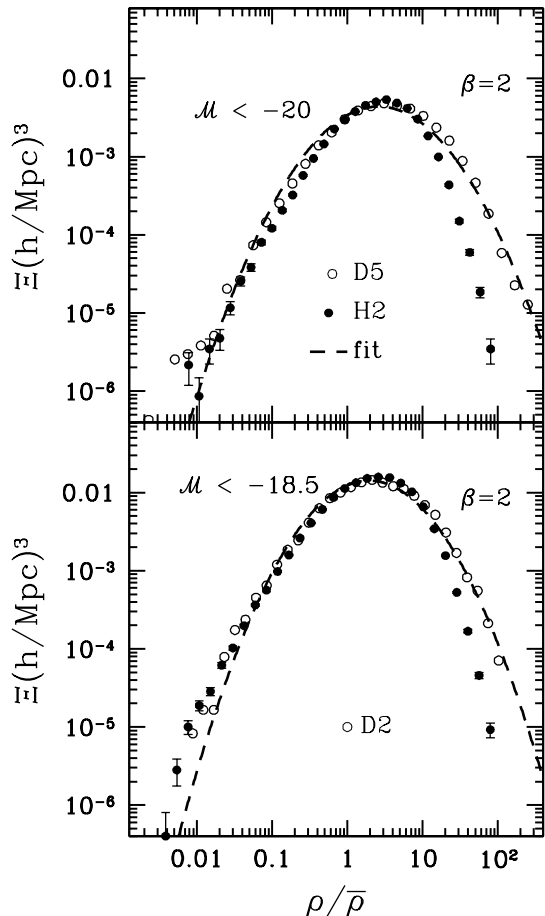


FIG. 5.— Distributions of local overdensities for the sample of mock (*filled circles*) and SDSS galaxies (*open circles*) in the magnitude ranges of  $\mathcal{M} < -20$  (*upper*) and  $\mathcal{M} < -18.5$  (*lower*) panels) in the  $\beta = 2$  model. The dashed line shows the log-normal fit to observations.

TABLE 2  
THE LOG NORMAL FUNCTION PARAMETERS OF  
THE LOCAL DENSITY DISTRIBUTIONS OF THE  
SDSS GALAXIES

$\mathcal{M}_{\text{min}}$	sample	$A(h^{-1}\text{Mpc})^{-3}$	$\mu$	$\sigma$
-18.5	D2	$4.53 \times 10^{-2}$	0.662	1.27
-20	D5	$1.47 \times 10^{-2}$	0.949	1.34
-20.5	D5	$7.44 \times 10^{-3}$	1.11	1.30
-21	D5	$2.76 \times 10^{-3}$	1.23	1.26

densities ( $\rho/\bar{\rho} < 10$ ) even though there is only one input parameter in our model. Late type galaxies dominate these regions. From these figures, it appears that the galaxy morphology depends only on the halo mass and does not directly depend on environment. But the number density analysis alone is not so sufficient to draw any definite conclusion of the environmental effect. We will further investigate this effect by comparing the luminosity functions of the SDSS with those of the mock galaxies in various environments in the next section. In the high density regions our model gives too few galaxies, which is probably due to the insufficient resolution of the simulation to maintain small subhalos within clusters and to the lack of gas physics.

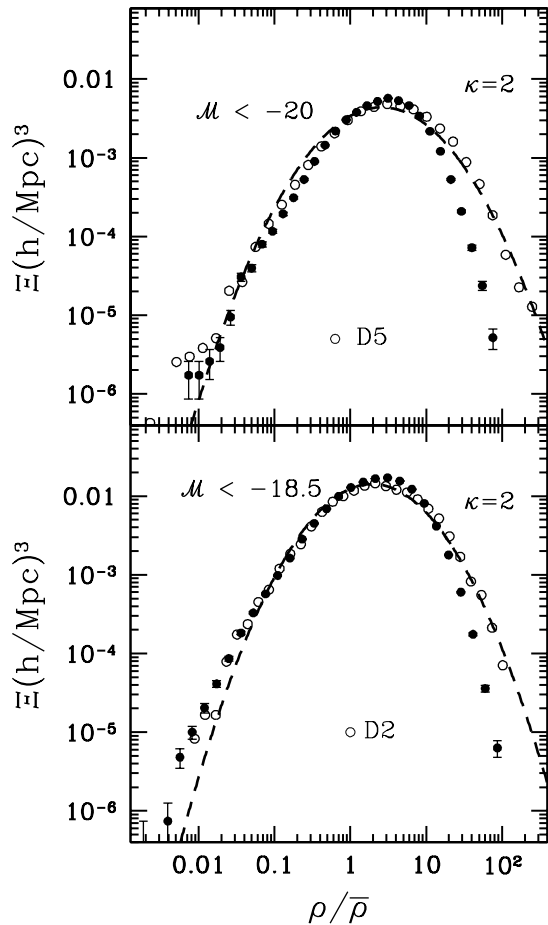


FIG. 6.— Similar to Fig. 5 but for the  $\kappa = 2$  model.

## 5. LUMINOSITY FUNCTION

There have been several works reporting the environmental dependence of the galaxy luminosity function (Park et al. 1994 and 2007a in observations and Mo et al. 2004 in the HOD model). It was found that the characteristic galaxy luminosity ( $L_*$ ) is an increasing function of the local density, and the faint-end slope ( $\alpha$ ) of the luminosity function is insensitive to the local density. However, Park et al. (2007a) used a spline kernel weighting to estimate local densities, and Mo et al. (2004) (also Cooray 2005) use a spherical top-hat filter of a constant radius. For a quantitative comparison between observations and models the same density estimation scheme is required.

In the previous section, we studied the one-point distribution of the local density at galaxy locations for each morphology sample of galaxies brighter than a certain absolute magnitude limit. In this section, we investigate the distribution of the absolute magnitude of early and late type galaxies located in different local density environment. This gives us environment and morphology-specific luminosity function of galaxies. In our galaxy morphology assignment scheme we only use the observed total luminosity function and the parameter  $\beta$  (or  $\kappa$ ), the ratio of luminosity (or mass) of the early and late types at a fixed mass (or luminosity). It will be interesting to see how accurately our model reproduces the observed luminosity functions at different local densities

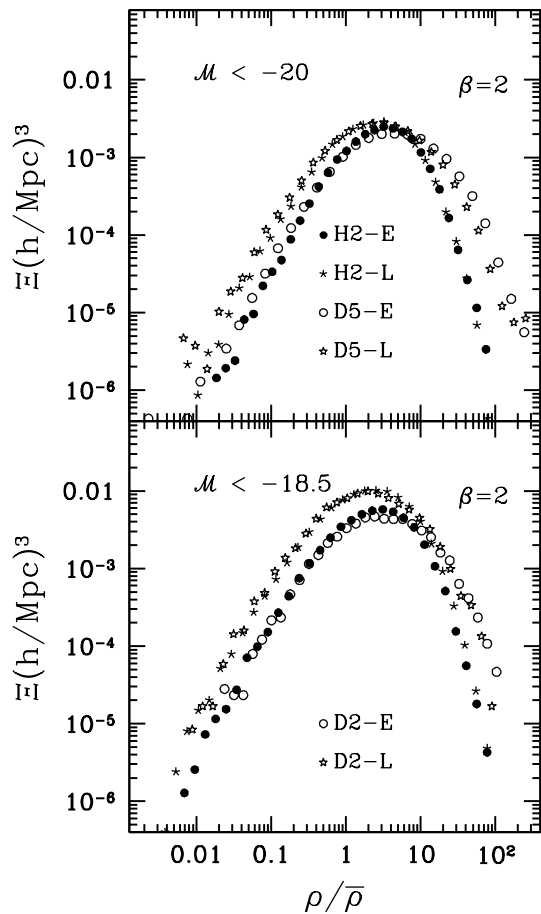


FIG. 7.— Local overdensity distributions for the two morphological types in the  $\beta = 2$  model. The distributions of local overdensity of mock and SDSS galaxies (D5 and D2) are shown for two magnitude-limit samples  $\mathcal{M} < -20$  (upper) and  $\mathcal{M} < -18.5$  (lower panels). Open circles and open stars mark the distributions of overdensity of the early type and late type SDSS galaxies. And filled circles and skeletal stars are those of mock galaxies for the corresponding types. We tag each panel with the magnitude criteria of the sample in the upper-left corner.

and for different morphological types. For this comparison we use the luminosity functions measured from the D3 sample of Park et al. (2007a) because this absolute magnitude-limited sample covers both bright and faint magnitudes well, relative to other volume-limited samples. The fitting of the measured luminosity functions to the Schechter formula is carried out by using the MINUIT<sup>7</sup> packages which employ the maximum likelihood method.

Figure 9 and 10 show the comparison of the luminosity functions in four different local density regions in the  $\beta = 2$  and  $\kappa = 2$  models. The resulting environment and morphology-specific luminosity function reproduces the observations surprisingly well. However, there are notable disagreements for two cases. At very high densities ( $\rho/\bar{\rho} > 10$ ) the abundance of faint early type galaxies are significantly low in the simulation. This is again probably due to the lack of small subhalos that were destroyed in high density environment. Another problem is seen at low densities ( $\rho/\bar{\rho} < 1$ ), where the early type galaxies are too few in the bright end of luminosity function.

<sup>7</sup> <http://wwwasdoc.web.cern.ch/wwwasdoc/minuit/minmain.html>

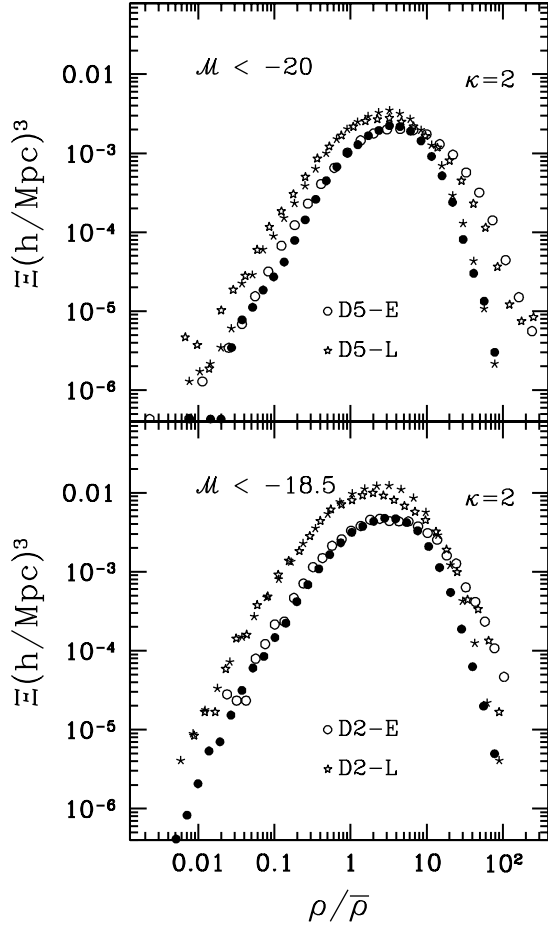


FIG. 8.— Same as Fig. 7 but for the  $\kappa = 2$  model.

It seems that the morphology transformation to bright early types in underdense regions through close interactions and mergers is more efficient in the nature than in our model (Park et al. 2008 for observational evidence). In the high density regions, the  $\kappa = 2$  model describes the number distribution of faint late type galaxies better than the  $\beta = 2$  model while this  $\kappa$  model shows a slight overestimation in the population of faint late types in the mean fields ( $0.4 < \log(\rho/\bar{\rho}) < 1$ ) compared to the observation.

Figure 11 and 12 compare the parameter of the Schechter function best fit to the SDSS data (open symbols) and simulated galaxy samples (filled symbols) as a function of local density in the  $\beta = 2$  and  $\kappa = 2$  models. The dependence of both  $\mathcal{M}_{T*}$  and  $\alpha$  on local density is qualitatively well-reproduced by the simulation. However, the characteristic magnitude  $\mathcal{M}_*$  of the early types is significantly fainter at  $\rho/\bar{\rho} < 2$  in the simulation. This is due to paucity of bright early type galaxies in low density regions, which is mentioned above. The parameter  $\alpha$  of the simulation is quite different from the observation at  $\rho/\bar{\rho} > 2$  for early type galaxies. This is again due to the flat faint end slope of the luminosity function of the simulated early type galaxies.

## 6. CENTRAL VELOCITY DISPERSION

Figure 13 shows the central velocity dispersion of early type galaxies in the D3 sample. The gray symbols with connecting lines are the relations between  $\sigma_v$  and the lo-

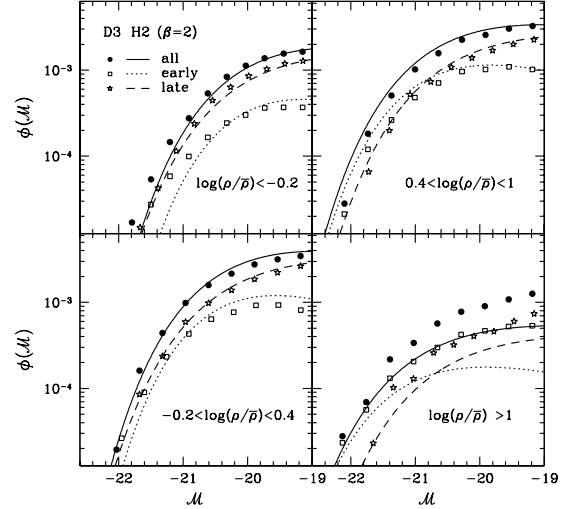


FIG. 9.— Luminosity functions of mock (*curves*) and SDSS (*symbols*) galaxies in the  $\beta = 2$  model. Each line shows the luminosity functions of the mock galaxies; *solid lines* for total, *dotted lines* for early type galaxies, and *dashed lines* for late type galaxies. For comparison, we show the luminosity densities of the SDSS subsamples divided by the same density cuts. The sample selection criteria are based on the log scale of local density and are written in the lower-right corner of each panel.

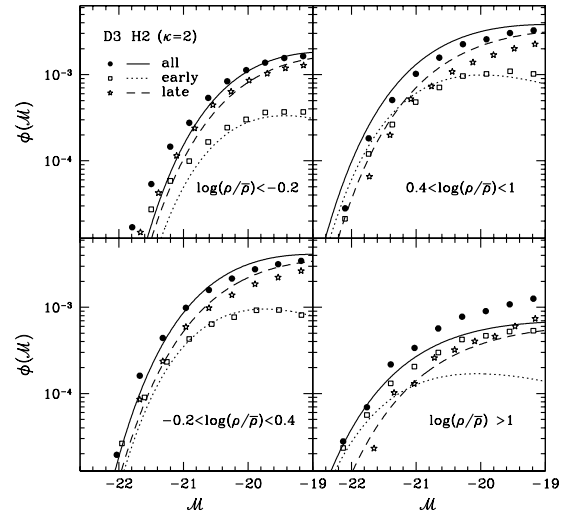


FIG. 10.— Similar to Fig. 9 but for the  $\kappa = 2$  model.

cal density for early type galaxies in four subsamples with absolute magnitude limits of  $-19.0 > \mathcal{M} > -19.3$  (bottom curve),  $-19.3 > \mathcal{M} > -20.1$ ,  $-20.1 > \mathcal{M} > -20.5$ , and  $\mathcal{M} < -20.5$  (top curve with filled circles). The curves delineate the median value of  $\sigma_v$  in each local density bin, which monotonically increases as luminosity increases. We also plot the scaled one-dimensional velocity dispersion of the early type mock galaxies with black symbols. Because the observed velocity dispersion is obtained by sampling the inner part ( $\leq 1''.5$ ) of the galaxy, we have to apply a scaling factor to the mock galaxy velocity dispersions. Because it is irrelevant in this paper to derive the exact value of the scaling factor and apply it to the related analysis, we make a rough estimation of the relation between  $\sigma_{los}$  and  $V_v$ , where  $\sigma_{los}$  is the line-of-sight aperture velocity dispersion and  $V_v$  is the virial velocity. According to Lokas & Mamon



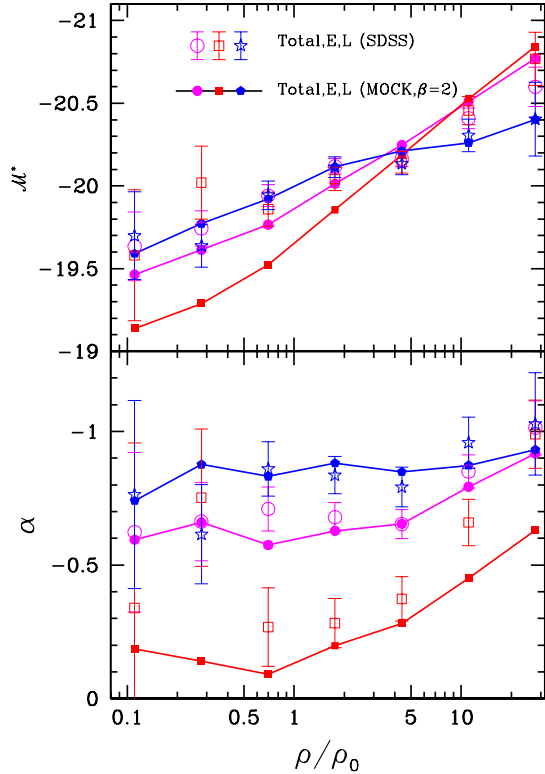


FIG. 11.— Dependence of the Schechter parameter values,  $\mathcal{M}^*$  (top) and  $\alpha$  (bottom panel), on the local density for the SDSS D3 (open symbols) and Mock (filled symbols) samples in the  $\beta = 2$  model. Circles mark the fitting values of full galaxy samples and boxes are for the early type samples. Open stars and filled hexagons are for the late types of the SDSS and mock samples, respectively. In this plot we add the error bars only to the SDSS fitting values and connect only the mock results with solid lines for clarity.

(2001), the resulting scaling ratio of the velocity dispersions,  $f_c (\equiv \sigma_{los}/V_v)$ , is

$$0.5 \lesssim f_c \lesssim 3 \quad (12)$$

for the acceptable ranges of the velocity anisotropy and the concentration parameter in  $0 < (r_a/R_v) < 1$ , where  $r_a$  is the comoving aperture radius. Here we assume that  $V_v = \sigma_v$ , where  $\sigma_v$  is the three-dimensional velocity dispersion and  $V_v \equiv \sqrt{2GM_v/R_v}$ . In the range of  $f_c$  written in equation (12), we simply set  $f_c = 0.8$  ( $\mathcal{M} < -20.5$ ),  $f_c = 1$  ( $-20.5 < \mathcal{M} < -20.1$ ),  $f_c = 1.1$  ( $-20.1 < \mathcal{M} < -19.3$ ), and  $f_c = 1.2$  ( $-19.3 < \mathcal{M} < -19.0$ ) to match for the mean amplitudes of velocity dispersions for each mock and SDSS sample pair. At a fixed luminosity the velocity dispersion of the early type mock galaxies increases as the local density increases for bright galaxies and the slopes are decreasing for the faint sample. It is reassuring that this trend is exactly the kind of phenomenon found in the observation (*gray symbols*). While the switch of the slope in the faintest SDSS samples is not clearly observed in the mock sample (it shows a nearly flat slope on the local environments), the change of the slope is similar to each other. Both observation and our model show that the mass-to-light ratio of the early type galaxies is a function of environment, and that this dependence in turn is a function of luminosity. The mass-to-light ratio of the early types decreases as the local density increases for galaxies brighter than about  $\mathcal{M}_*$ , but increases for those fainter than about  $\mathcal{M}_* + 1$ .

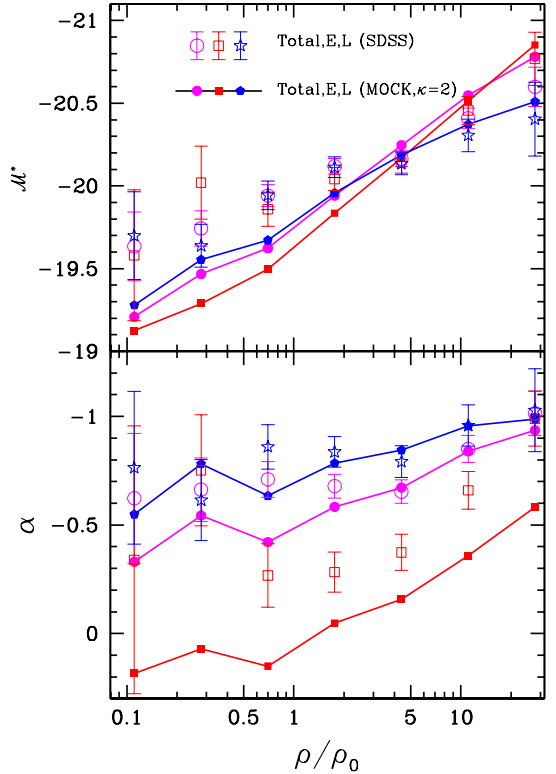


FIG. 12.— Similar to Fig. 11 but for  $\kappa = 2$  model

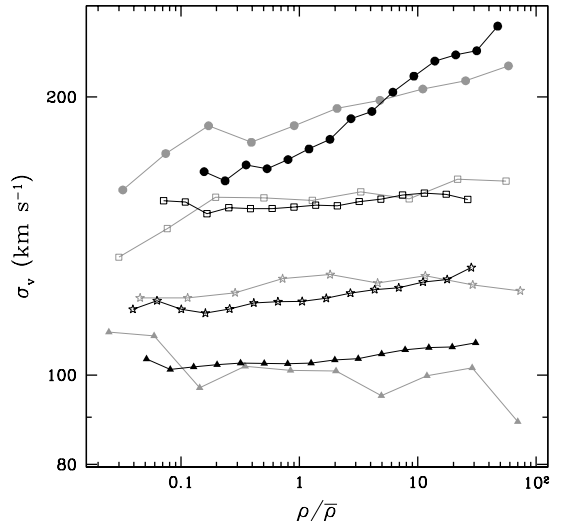


FIG. 13.— Median distribution of central velocity dispersions of SDSS (gray symbols) galaxies and scaled one-dimensional velocity dispersions of Mock (black symbols) galaxies of early types in the four magnitude-limit samples divided by four magnitude cuts. The magnitude ranges of the subsamples are  $\mathcal{M} < -20.5$ ,  $-20.5 < \mathcal{M} < -20.1$ ,  $-20.1 < \mathcal{M} < -19.3$ , and  $-19.3 < \mathcal{M} < -19$  from top to bottom lines, respectively.

## 7. SUMMARY & CONCLUSION

We have proposed a model to assign galaxy luminosity and morphology to the dark subhalos directly identified in cosmological N-body simulations. It is assumed that the galaxy luminosity is a monotonic function of its host halo mass. In the  $\kappa$  model we assume that the halo masses of early and late type galaxies of equal luminos-

ity have a constant ratio. Another alternative model is the  $\beta$  model which assumes the constant luminosity ratio between equal-mass galaxies of different types. This model has been proposed by Marinoni & Hudson (2002) who found that the observed  $B$ -band luminosity function of galaxies can be reproduced from the PS function assuming double power-law mass-to-light ratios and derived halo occupation numbers. It has been expanded by Vale & Ostriker (2004, 2006) who adopted the satellite halo mass functions and directly link subhalos to the observed galaxies. In this paper, we have introduced the ratio of luminosity of the early and late morphological type galaxies at a given halo mass, and derived type-specific mass-to-light ratios as a function of subhalo mass. They are used to assign luminosity and morphology to subhalos. The mass-to-light ratio of the early type galaxies derived in this way has a minimum value of  $\Upsilon_u \simeq 100$  at the scale of  $M_u \simeq 3 \times 10^{11} h^{-1} M_\odot$  in the  $\beta = 2$  model. The mass-to-light ratio starts to exponentially increase below  $M_u$  and increases in a power law above  $M_u$ .

We use the large-scale background galaxy number density as an environmental parameter. The smooth galaxy density field is obtained by using the adaptive spline kernel which enabled us to resolve crowded regions well. The local density distribution of the SDSS galaxies is well described by the log normal function. The obtained log normal parameter values indicate that brighter galaxies tend to locate in dense regions. The local density distribution of the simulated galaxies is quite similar to that of the SDSS galaxies in voids and moderate-density regions for both morphological types. The underestimation of galaxy population in clusters is thought to be due to the evaporation of subhalos by the dynamical friction and tidal stripping. This can also explain the discrepancy in the luminosity function of the early type galaxies in high density regions.

Recently, Gott et al. (2006) measured the genus statistic from a large sample of the SDSS galaxies and compared it with those of mock galaxies created by the three distinctive methods such as the semi-analytic galaxy formation model applied to the Millennium run (Springel et al. 2005), a hydrodynamic simulation, and the subhalo-galaxy correspondence model adopted in this paper. It was found that the observed topology of large scale structure was best reproduced by the subhalo-galaxy correspondence model even though other models were also consistent with the observation. However, the observed topology was marginally inconsistent with all simulations in the sense that it showed a strong meatball topology at the significance level of  $2.5\sigma$  at the scale studied. The prominence of the isolated high density regions in the observation seems to be due to the Sloan Great Wall which was a dominant structure in the sam-

ple analyzed.

We have found an impressive agreement between our simulated galaxies and the SDSS galaxies in the dependence of the central velocity dispersion on the local density and luminosity. The early type galaxies tend to have higher  $\sigma_v$  or higher mass in high density regions at a given luminosity when they are brighter than about  $\mathcal{M}_*$ . In other words, these bright galaxies tend to become relatively fainter in high density regions at a given halo mass. This interesting dependence of the mass-to-light ratio on environment was successfully reproduced by our subhalo-galaxy correspondence model of galaxy formation. A more detailed study of this phenomenon will be presented in a forthcoming paper.

CBP acknowledges the support of the Korea Science and Engineering Foundation (KOSEF) through the Astrophysical Research Center for the Structure and Evolution of the Cosmos (ARCSEC). Funding for the SDSS and SDSS-II has been provided by the Alfred P. Sloan Foundation, the Participating Institutions, the National Science Foundation, the U.S. Department of Energy, the National Aeronautics and Space Administration, the Japanese Monbukagakusho, the Max Planck Society, and the Higher Education Funding Council for England. The SDSS Web Site is <http://www.sdss.org/>.

The SDSS is managed by the Astrophysical Research Consortium for the Participating Institutions. The Participating Institutions are the American Museum of Natural History, Astrophysical Institute Potsdam, University of Basel, Cambridge University, Case Western Reserve University, University of Chicago, Drexel University, Fermilab, the Institute for Advanced Study, the Japan Participation Group, Johns Hopkins University, the Joint Institute for Nuclear Astrophysics, the Kavli Institute for Particle Astrophysics and Cosmology, the Korean Scientist Group, the Chinese Academy of Sciences (LAMOST), Los Alamos National Laboratory, the Max-Planck-Institute for Astronomy (MPIA), the Max-Planck-Institute for Astrophysics (MPA), New Mexico State University, Ohio State University, University of Pittsburgh, University of Portsmouth, Princeton University, the United States Naval Observatory, and the University of Washington.

The authors would like to acknowledge the use of the linux cluster, QUEST, at the Korea Institute for Advanced Study (KIAS). Its huge computing power is indispensable for the study, and we thank the system managers for their efforts in providing a stable and comfortable computation resources during the simulation and subsequent analysis.

## REFERENCES

- Abazajian, K., Zheng, Z., Zehavi, I., Weinberg, D.H., Frieman, J.A., Berlind, A.A., Blanton, M.R., Bahcall, N.A., Brinkmann, J., Schneider, D.P., & Tegmark, M. 2005, *ApJ*, 625, 613
- Baugh, C.M. 2006, *Report on Progress in Physics*, 69, 3101
- Berlind, A.A. & Weinberg, D.H. 2002, *ApJ*, 575, 587
- Blanton et al. 2001, *AJ*, 121, 2358
- Blanton, M.R. & Roweis, S. 2007, *ApJ*, 133, 754
- van den Bosch, F.C., Yang, X., & Mo, H.J. 2003, *MNRAS*, 340, 771
- Cervantes-Sodi, B., Hernandez, X., Park, C., & Kim, J. 2007, [arXiv/0712.0843](http://arXiv.org/abs/0712.0843)
- Cole, S., Aragon-Salamanca, A., Frenk, C.S., Navarro, & Zepf, S.E. 1994, *MNRAS*, 271, 781
- Conroy, C.C., Wechsler, R.H., & Kravtsov, A.V. 2006, *ApJ*, 647, 201
- Cooray, A. 2005, *MNRAS*, 363, 337
- Dubinski, J., Kim, J., Park, C., & Humble, R. 2003, *New Astronomy*, 9, 111
- Eke, V.R., Baugh, C.M., Cole, S., Frenk, C.S., & Navarro, J.F. 2006, *MNRAS*, 370, 1147
- Evans, N.W. & Wilkinson, M.I. 2000, *MNRAS*, 316, 929

- Gao, L., De Lucia, G., White, S.D.M., & Jenkins, A. 2004, MNRAS, 352, L1
- Gott, J.R., Hambrick, D.C., Vogeley, M.S., Kim, J., Park, C., Choi, Y.-Y., Cen, R., Ostriker, J.P., & Nagamine, K. 2006, ApJ, in press
- Harten, A. 1997, Journal of Computational Physics, 135, 260
- Hernandez, X., Park, C., Cervantes-Sodi, B., & Choi, Y.-Y. 2007, MNRAS, 375, 163
- Hernquist, L. & Katz, N. 1989, ApJS, 70, 419
- Jing, Y.P., Mo, H.J., & Börner, G. 1998, ApJ, 494, 1
- Kauffmann, G., Nusser, A., & Steinmetz, M. 1997, MNRAS, 286, 795
- Kim, J. & Park, C. 2006, ApJ, 639, 600
- Kravtsov, A.V., Berlind, A.A., Wechsler, R.H., Klypin, A.A., Gottlöber, S., Allgood, B., & Primack, J.R. 2004, ApJ, 609, 35
- Lokas, E.L. & Mamon, G.A. 2001, MNRAS, 321, 155
- Madelbaum, R., Seljak, U., Kauffmann, G., Hirata, C.M., & Brinkmann, J. 2006, MNRAS, 368, 715
- Marinoni, C. & Hudson, M. 2002, ApJ, 569, 101
- Mo, H.J., Yang, X., van den Bosch, F.C., & Jing, Y.P. 2004, MNRAS, 349, 205
- Monaghan, J.J. 1992, Annual Review of Astronomy and Astrophysics, 30, 543
- Heitmann, K., Ricker, P.M., Warren, M.S., & Habib, S. 2006 ApJS, 160, 28
- Ostriker, J.P., Nagamine, K., Cen, R., & Fukugita, M. 2003, ApJ, 597, 1
- Park, C., Kim, J., & Gott, J.R. 2005, ApJ, 633, 1
- Park, C., Choi, Y.-Y., Vogeley, M.S., Gott, J.R., Kim, J., Hikage, C., Matsubara, T., Park, M.-G., Suto, Y., & Weinberg, D.H. 2005, 633, 11
- Park, C., Choi, Y.-Y., Vogeley, M., Gott, J.R., & Blanton, M.R. 2007, ApJ, 658, 898
- Park, C., Gott, J.R., & Choi, Y.-Y. 2008, ApJ, in press
- Sakamoto, T., Chiba, M., & Beers, T.C. 2003, A&A, 397, 899
- Seljak, U. 2000, MNRAS, 318, 203
- Shankar, F., Lapi, A., Salucci, P., Zotti, G.De, & Danese, L. 2006, ApJ, 643, 14
- Shaw, L.D., Weller, J., Ostriker, J.P., & Bode, P. 2006, ApJ, 646, 815
- Sheth, R.K. & Tormen, G. 1999, MNRAS, 308, 119
- Sheth, R.K., Mo, H.J., & Tormen, G. 2001, MNRAS, 323, 1
- Springel, V., White, S.D.M., Tormen, G., & Kauffmann, G. 2001, MNRAS, 328, 2001
- Springel, V. et al. 2005, Nature, 435, 629
- Tasker, E.J. & Bryan, G.L. 2006, ApJ, 641, 878
- Thacker, R.J., Tittley, E.R., Pearce, F.R., & Couchman, H.M.P. 2000, MNRAS, 319, 619
- Tinker, J.L., Weinberg, D.H., Zheng, Z., & Zehavi, I. 2005, ApJ, 631, 41
- Vale, A. & Ostriker, J.P. 2004, MNRAS, 353, 189
- Vale, A. & Ostriker, J.P. 2006, MNRAS, 371, 1173
- Vale, A. & Ostriker, J.P. 2007, astro-ph/0701096
- Weinberg, D.H., Colombi, S., Dave, R., & katz, N. 2006, astro-ph/0604393
- Weller, J., Ostriker, J.P., Bode, P., & Shaw, L. 2005, MNRAS, 364, 823
- Zehavi, I., et al. for the SDSS Collaboration 2004, ApJ, 608, 16
- Zentner, A.R., Berlind, A.A., Bullock, J.S., Kravtsov, A.V., & Wechler, R.H. 2005, ApJ, 624, 505
- Zheng, Z., Berlind, A.A., Weinberg, D.H., Benson, A.J., Baugh, C.M., Cole, S.C., Dave, R., Frenk, C.S., Katz, N., & Lacey, C.G. 2005, ApJ, 633, 809
- Zheng, Z., Coil, A.L., & Zehavi, I. 2007, astro-ph/0703457
- Yang, X., Mo, H.J., & van den Bosch, F.C. 2003, MNRAS, 339, 1080